Letter

Theory of three-terminal Andreev spin qubits

Aleksandr Svetogorov,[1,*] Kiryl Piasotski,[2,3] Wolfgang Belzig,[1] and Mikhail Pletyukhov[4]
[1] *Universität Konstanz, 78457 Konstanz, Germany*
[2] *Institut für Theorie der Kondensierten Materie (TKM), Karlsruher Institut für Technologie, 76131 Karlsruhe, Germany*
[3] *Institut für Quanten Materialien und Technologien (IQMT), Karlsruher Institut für Technologie, 76021 Karlsruhe, Germany*
[4] *Institut für Theorie der Statistischen Physik, RWTH Aachen, 52074 Aachen, Germany*

(Received 19 November 2024; accepted 15 September 2025; published 26 September 2025)

In this Letter, we introduce a next generation of Andreev spin qubits—three-terminal Andreev spin qubits. These qubits outperform two-terminal devices in the speed of two-qubit gates, benefiting from enhanced spin splitting. Our theoretical analysis reveals increased tunability and interqubit coupling mediated by the supercurrent. Furthermore, it provides a comprehensive explanation for the results of a recent experiment on a three-terminal device [M. Coraiola *et al.*, Phys. Rev. X **14**, 031024 (2024)]. We identify the optimal operational regime for single- and two-qubit gates. Moreover, our concise theoretical framework for the equilibrium multiterminal Josephson effect offers significant potential for exploring nontrivial physics in the artificial dimensions of superconducting phase differences——a rapidly growing field of research.

DOI: 10.1103/55xn-c574

Introduction. Andreev spin qubits (ASQs) have been proposed in a theoretical work [1] as a way to combine electron spins in localized states that can maintain coherence on long timescales [2,3] and strong long-range coupling via Cooper pairs condensate. Coupling between an electron spin and supercurrent is achieved by spin-orbit interactions (SOI) [4–10]; such hybridized spin is usually referred to as pseudospin. The first ASQ has recently been developed [11] in a semiconducting nanowire, where SOI lift the degeneracy of two states of a quasiparticle localized in an Andreev bound state (ABS) between two superconducting leads. Further experiments were performed in a semiconducting quantum dot (QD), where a combination of SOI and magnetic field allowed for a visible splitting as well as a long-range coupling between two ASQs [12,13]. Nevertheless, to speed up two-qubit gates, stronger spin splitting is required. Therefore, we suggest an improved design of an ASQ—a three-terminal Andreev spin qubit (TASQ)—that demonstrates enhanced spin splitting of the ABS [14,15].

In our work, we harness a powerful Green's function formalism [16–27] developed further in a recent theoretical work [28]. Such an approach allows us to establish the nontrivial properties of a three-lead setup in comparison to a Josephson junction with two leads. We further develop the ideas put forth in a theoretical work [14], such as the enhanced phase-dependent spin splitting of the bound states and changes in the ground-state fermion parity.

*Contact author: aleksandr.svetogorov@uni-konstanz.de

Our model captures features observed in a recent experiment [15] and allows us to propose an optimal regime for the qubit operation. Our findings combined with experimental evidence [15] suggest that the TASQ is a feasible device that overcomes one of the main disadvantages of a two-terminal ASQ—the weak splitting of ABSs. The higher connectivity of the TASQ as a circuit node enables a wider range of multiqubit architectures, leveraging the robust long-distance supercurrent-mediated interqubit coupling.

Results: Quantum model and its spectrum. In this section, we present a simple low-energy description of three-terminal Josephson junctions in two-dimensional electron gas with spin-orbit interaction. We begin by noting that the dominant portion of the current flowing between the superconductors through the semiconducting plate is transmitted via one-dimensional ballistic channels connecting the contact points. Further leveraging the techniques of Ref. [28] to integrate these channels out enables the construction of an effective low-energy model in the space of the three contact points, akin to the empirical quantum dot model proposed in Ref. [10].

As is earlier anticipated, we can model the semiconducting plate connecting the three superconducting electrodes with a triangle made up of one-dimensional ballistic channels that link the contact points of the electrodes [see Fig. 1(a)]. It is crucial to note that in the semiconducting part of the system, the Rashba Hamiltonian, traditionally written in the form $H_R = \alpha_R(-k_x\sigma_y + k_y\sigma_x)$, describes the spin-orbit coupling in the two-dimensional electron gas. Our convention, however, is to represent it as $\alpha_R \vec{k}\cdot\vec{\sigma}$, with $\vec{k} = k_x\vec{e}_x + k_y\vec{e}_y$, assuming the rotation of the Pauli matrices $\sigma_y \to -\sigma_x$, $\sigma_x \to \sigma_y$. This convention facilitates a determination of the one-dimensional projections $H_R^{(jj')} = \alpha_R k\, \vec{e}^{\,(jj')}\cdot\vec{\sigma}$ of H_R onto the triangle's sides by means of identifying $\vec{e}^{\,(21)} = \vec{e}_x$, $\vec{e}^{\,(32)} = \mathcal{R}(\beta-\pi)\vec{e}_x$, and $\vec{e}^{\,(13)} = \mathcal{R}(\pi-\beta)\vec{e}_x$, where $\beta = \arccos(\frac{L}{2L'})$ and $\mathcal{R}$ is the rotation matrix with the corresponding angle argument. The equivalent representation $H_R^{(jj')} = \alpha_R k\, U^{(jj')}\sigma_x U^{(jj')\dagger}$,

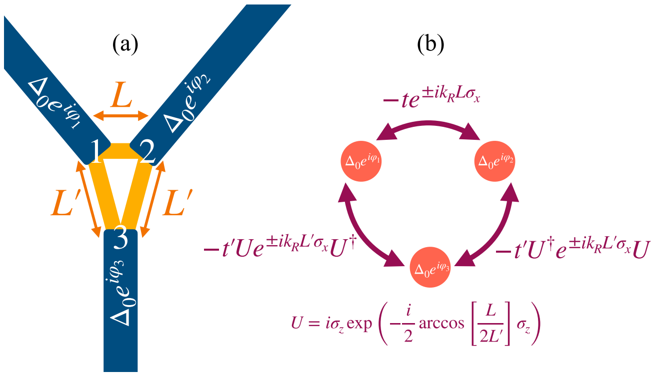

FIG. 1. Sketch of the effective model's configuration. As illustrated in (a), the effective model replaces the semiconducting plate (where the superconducting electrodes connect) with three quantum wires linking the contacts (see SM [29] for details). By further integrating the extended components of the system and projecting onto the Fermi surface, we can establish (see SM [29]) an effective three-site model based on the contact points of the original setup, as described by Eq. (1) and schematically depicted in (b). Additionally, the spin-momentum locking from the original model results in rotations of spin-dependent hopping amplitudes as one moves from one contact to another, as is further schematically indicated in (b).

with $U^{(21)} = 1$ and $U^{(32)} = U^{(13)\dagger} = e^{\frac{i}{2}(\pi-\beta)\sigma_z} \equiv U$, proves to be especially useful in the derivation of the effective model.

Therefore, the SOI in the original semiconducting plate is assumed to be constant throughout the sample, which results in the spin-orbit vector in the effective three-channel model having different angles to the the propagation directions $\vec{e}^{\,(jj')}$ along the segments from the contact j' to the contact j ($j, j' = 1, 2, 3$). For simplicity, we will consider an isosceles triangle with a horizontal side of the length L and two oblique sides of the length L'. We assume that both the s-wave superconductors and the semiconductors have spatially uniform parameters. In particular, the energy gap parameter Δ_0 has the same value in all superconducting leads j, and their phases φ_j can be tuned by external fluxes. In addition, we assume that an effective electron mass m_W is the same in the semiconducting and superconducting parts of the system.

In the next step, we integrate out the extended components of the effective wire model described above [and sketched in Fig. 1(a)] mapping it onto an effective three-site low-energy model [see Fig. 1(b)], where sites represent the zero-dimensional contact points, marked by indices j. Referring interested readers to the details of our microscopic derivation in Sec. 1 of the Supplemental Material (SM) [29], we state the following effective 12×12 Nambu Hamiltonian, formulated in the combined space of spin, particle-hole, and contact-point indices, that describes the low-lying excitations in the discussed device:

$$h_{\rm eff} = \begin{pmatrix} \epsilon\tau_z + \Delta_0 e^{\frac{i}{2}\varphi_1\tau_z}\tau_x e^{-\frac{i}{2}\varphi_1\tau_z} & -t\tau_z e^{i\varphi_{SO}\sigma_x} & -t'\tau_z U^\dagger e^{-i\varphi'_{SO}\sigma_x} U \\ -t\tau_z e^{-i\varphi_{SO}\sigma_x} & \epsilon\tau_z + \Delta_0 e^{\frac{i}{2}\varphi_2\tau_z}\tau_x e^{-\frac{i}{2}\varphi_2\tau_z} & -t'\tau_z U e^{i\varphi'_{SO}\sigma_x} U^\dagger \\ -t'\tau_z U^\dagger e^{i\varphi'_{SO}\sigma_x} U & -t'\tau_z U e^{-i\varphi'_{SO}\sigma_x} U^\dagger & \epsilon'\tau_z + \Delta_0 e^{\frac{i}{2}\varphi_3\tau_z}\tau_x e^{-\frac{i}{2}\varphi_3\tau_z} \end{pmatrix}. \tag{1}$$

The model's on-site energy ϵ, ϵ' and hopping t, t' parameters are obtained from the Fermi-level projections of the full system's Green's function, which is evaluated at the corresponding spatial points. The unitary matrix $U = i\sigma_z e^{-\frac{i}{2}\beta\sigma_z}$ takes into account the above-described direction's change of the quasiparticle propagation at each contact. The spin-orbit phases $\varphi_{SO} = k_R L$ and $\varphi'_{SO} = k_R L'$, expressed in terms of the Rashba momentum $k_R = m_W\alpha_R$, are accumulated during the propagation through the legs of the lengths L and L'.

Now it is appropriate to discuss the domain of validity of the low-energy theory presented above. In the experiment, the observed spectrum consisted of a vast number of low-transparency channels and, most importantly, a single high-transparency (ballistic) channel per pair of contacts—giving rise to the lowest pair of pseudo-spin-split Andreev bound states (ABS) studied in this work. As our model aims to accurately describe these specific low-energy modes (i.e., the lowest pair, not the higher-lying low-transparency channels), the discussed Hamiltonian accomplishes this task. This also justifies why we model the two-dimensional (2D) semiconductor plateau as three ballistic channels connecting each pair of superconducting contacts. This can be formally understood through a semiclassical argument: the dominant path between any two contacts is the least-action path—a straight line. It may be of interest to enhance the prominence of this channel, which could be achieved using a recently developed gating technique [30].

The correct interpretation of the model is that it is written in the basis of the three lowest-energy Andreev bound states at the three superconductor (SC)/semiconductor interfaces (referred to as contact points), each spatially attenuated over approximately a coherence length into the SC terminals. These Andreev bound states then hybridize in a non-Abelian fashion—i.e., with spin- and particle-hole-space-dependent coupling—as prescribed by our Hamiltonian in Eq. (1).

To justify the presence of only one bound state per contact, as well as the semiclassical picture outlined above, we rely on the so-called short-junction regime, defined by the following experimentally relevant hierarchy of length scales:

$$\frac{1}{\sqrt{2m\Delta}} \simeq \frac{v_{F,S}}{\Delta} > \max\{L, L'\} \geqslant k_R^{-1}. \tag{2}$$

Indeed, the junction used in the experiment was appreciably smaller than the superconducting coherence length, but still long enough to allow at least one spin precession to occur during transport.

The effective Hamiltonian (1) possesses various symmetries, which explain features of its spectrum to be discussed in the following. First of all, $h_{\rm eff}(\{\varphi_j\})$ possesses the particle-hole symmetry $C = \tau_y\sigma_y K$, with K denoting complex conjugation. It relates the Hamiltonian to itself at each fixed set of the phases $\{\varphi_j\}$,

$$Ch_{\text{eff}}(\{\varphi_j\})C^{-1} = -h_{\text{eff}}(\{\varphi_j\}). \tag{3}$$

The time-reversal operator $T = i\sigma_y K$, such that $T^2 = -1$, relates h_{eff} evaluated at the phases $\{\varphi_j\}$ to its time-reversal partner at $\{-\varphi_j\}$,

$$Th_{\text{eff}}(\{\varphi_j\})T^{-1} = h_{\text{eff}}(\{-\varphi_j\}). \tag{4}$$

This symmetry implies the twofold Kramers degeneracy of a spectrum at the *time-reversal invariant phases* $\varphi_j = 0, \pm\pi$.

Moreover, the Hamiltonian (1) conserves the pseudospin operator,

$$\Sigma = \mathcal{U}\frac{U_{SO} - \frac{1}{2}\text{tr}[U_{SO}]}{2i\sqrt{1 - \frac{1}{4}(\text{tr}[U_{SO}])^2}}\mathcal{U}^\dagger = \Sigma^\dagger, \quad \Sigma^2 = \frac{1}{4}, \tag{5}$$

where $U_{SO} = e^{i\varphi_{SO}\sigma_x}(Ue^{i\varphi'_{SO}\sigma_x}U^\dagger)(U^\dagger e^{i\varphi'_{SO}\sigma_x}U)$ is the total non-Abelian closed-loop spin-orbit phase accumulated along the triangle's circumference, and $\mathcal{U} = \text{diag}\{1,\ e^{-i\varphi_{SO}\sigma_x}U_{SO},\ U^\dagger e^{i\varphi'_{SO}\sigma_x}U\}$ is a unitary transformation acting trivially in the particle-hole space: $[\Sigma, \tau_{x,y,z,0}] = 0$. We refer to Sec. 2 of the SM [29] for the explicit demonstration of the commutation, $[\Sigma, h_{\text{eff}}(\{\varphi_j\})] = 0$. It is important to note that the pseudospin conservation generally holds for arbitrary triangular geometry, not just for the presently discussed isosceles case, with a general expression for Σ being more involved than in Eq. (5).

The pseudospin conservation implies that each ABS is characterized by the pseudospin quantum number ($+\frac{1}{2}$ or $-\frac{1}{2}$), and two ABSs with opposite pseudospin values have a protected crossing. Moreover, a holelike ABS has an opposite pseudospin value of its particlelike ABS partner—this follows from the anticommutation $\{C, \Sigma\} = 0$. One should note that to operate the qubit, one requires direct transitions between the pseudo-spin-split Andreev levels, which implies breaking of pseudospin conservation. That can be achieved by the direct gate voltage drive because electron dipole spin resonance (EDSR) [5,31–34] explicitly breaks pseudospin conservation, or by magnetic field, etc.

Models belonging to this symmetry class (three superconducting contacts attached to a semiconducting island with spin-orbit coupling) may host zero-energy eigenstates. In Ref. [14], the necessary condition for the existence of such eigenstates has been derived in the framework of the scattering matrix approach. It states that the interior of a triangle formed by the points $e^{i\varphi_1}$, $e^{i\varphi_2}$, $e^{i\varphi_3}$, which lie on the unit circle in the complex plane, must contain the circle's center. In Sec. 3 of the SM [29], we derive this condition for a spectrum of the effective Hamiltonian (1) by analyzing possibilities to satisfy the equation $\det[h_{\text{eff}}(\{\varphi_j\})] = 0$.

Applying the necessary condition for the choice of the phases $\varphi_3 = 0$, $\varphi_1 = -\varphi_2 \equiv \varphi$, we deduce that zero-energy states may only exist at $\varphi \in [\frac{\pi}{2}, \frac{3\pi}{2}]$. Plotting the spectrum of $h_{\text{eff}}(\{\varphi, -\varphi, 0\}) \equiv h_{\text{eff}}(\varphi)$ versus φ in Fig. 2, we observe that the zero-energy states do occur at the spin-orbit phase value $\varphi_{SO} = 2.2$. Since the spectrum is particle-hole symmetric, a pair of two crossings at zero energy occurs on the interval of φ between $\frac{\pi}{2}$ and π. The two crossings coalesce and disappear, as the parameter φ_{SO} is continuously cranked up to the value 2.6.

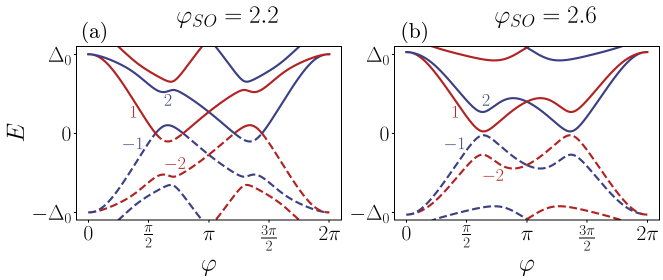

FIG. 2. The example of the energy spectrum of the effective Hamiltonian of Eq. (1) for the case of an isosceles triangle $L = 0.3L'$ with $\varphi_1 = -\varphi_2 = \varphi$, $\varphi_3 = 0$, $t = 10t'/3 = 0.7\Delta_0$, $\epsilon = 10\epsilon'/3 = 0.35\Delta_0$, and two distinct values of the spin-orbit angle $\varphi_{SO} = 0.3$, $\varphi'_{SO} = 2.2,\ 2.6$. Red and blue lines represent two different pseudospin projections, while solid and dashed lines distinguish particlelike and holelike solutions. Note that the effective Hamiltonian provides quantitatively accurate results only in the vicinity of zero energy. We index two states closest to zero energy by indices 1 and 2 for particlelike solutions and -1, -2 for their holelike counterparts.

In addition to the zero-energy states at $\varphi < \pi$, we also have their symmetric partners at $\varphi > \pi$. This happens due to the above-made special choice of phases, which leads to an emergent symmetry of the spectrum concerning its reflection about the $\varphi = \pi$ point. Formally, this symmetry is expressed in terms of the unitary operator $\Pi = \sigma_y R$, with $\Pi^2 = 1$,

$$\Pi h_{\text{eff}}(\varphi - \pi)\Pi^{-1} = h_{\text{eff}}(\pi - \varphi), \tag{6}$$

where the matrix

$$R = \begin{pmatrix} 0 & 1 & 0 \\ 1 & 0 & 0 \\ 0 & 0 & 1 \end{pmatrix} \tag{7}$$

geometrically reshuffles the contacts 1 and 2. It is also remarkable to note the emergence of two more symmetries supporting the spectral properties at a fixed value of φ: (a) the anti-unitary time-reversal-like symmetry $\tilde{T} = -i\Pi T = RK$, with $\tilde{T}^2 = 1$,

$$\tilde{T}h_{\text{eff}}(\varphi)\tilde{T}^{-1} = h_{\text{eff}}(\varphi), \tag{8}$$

and (b) the unitary chiral symmetry $S = C\tilde{T} = \tau_y\sigma_y R$,

$$Sh_{\text{eff}}(\varphi)S^{-1} = -h_{\text{eff}}(\varphi). \tag{9}$$

We find that the spectrum of our model is in good qualitative agreement with the low-energy spectrum recently observed in the experiment [15]. In particular, the phase dispersion of the lowest pair of spin-orbit split Andreev levels is described quite accurately, and we propose to utilize it for the realization of a TASQ. The values of φ_{SO} used in the model are compatible with the sample sizes (300×250 nm) and estimated SOI length $k_R^{-1} \approx 150$ nm.

To achieve an optimal regime for a single TASQ operation, the pair of positive-energy quasiparticle states should, on one hand, lie deep below Δ_0, and, on the other hand, should feature a sufficiently large pseudospin splitting. In Fig. 2, we see that in the presence of zero-energy crossings, a holelike state turns into a particlelike state between the two successive crossings on the interval $0 < \varphi < \pi$ (and symmetrically on the interval $\pi < \varphi < 2\pi$) retaining its pseudospin value. Thus, the two lowest positive-energy quasiparticle states between the crossings have the same pseudospin value, which is unfavorable for the realization of the ASQ. Ramping up the spin-orbit phase φ_{SO} (see Fig. 2), we achieve the coalescence of the two crossings and their subsequent disappearance. After that, the two lowest positive-energy states near $\varphi \approx \frac{2\pi}{3}$ feature the opposite values of pseudospin, as well as a sufficiently large pseudospin splitting. In addition, both phase dispersions (blue and red) feature local minima near this phase value, which protects the corresponding transition frequency against noise. This regime appears to be optimal for a single TASQ operation. Note that for two-qubit operations, one needs to detune from that optimal point to have finite supercurrent (as the local minima of the phase dispersion correspond to zero supercurrent).

Driving transitions and coupling two qubits. In realistic semiconductor platforms, the presence of electric dipole spin resonance (EDSR) [31–33], i.e., a strong coupling between spin and electric fields, dynamically breaks the pseudospin conservation and enables transitions between the lowest pair of pseudo-spin-split ABSs [5,12,13]. An alternative route to lifting this symmetry is to apply a static magnetic field, which breaks the pseudospin symmetry explicitly and likewise permits driving the transition. We refer the interested reader to Secs. 4–6 of the SM [29], where both mechanisms are discussed in the context of our three-terminal device. Both methods allow for the implementation of all necessary single-qubit gates [1,5]. Then, only a CNOT gate with two qubits is required to enable universal quantum computation [35,36].

One can couple two tripod junctions via a superconducting circuit. Owing to the gapped nature of excitations in superconducting wires connecting the qubits, the direct overlap of ABS wave functions is exponentially suppressed. The leading-order interaction between the qubits is provided by the fluctuations of the phase fields shared by the junctions [5,13] (often referred to as inductive coupling) and leads to Ising-type interaction between two pseudospins. A similar Ising-type interaction can be achieved with a single transmission line connecting two qubits via plasmons [37]; see Sec. 7 of the SM [29] for details. This coupling is sufficient to perform a CNOT gate between two qubits [1,5]. Two qubits can be arranged in a circuit similarly to the configuration used in two-terminal qubit setups [12,13]. Each TASQ includes an additional loop threaded by a magnetic flux, which serves as a convenient control knob for tuning the qubit energy levels. The three-terminal geometry allows for a controlled enhancement of interqubit coupling, which provides a way to speed up two-qubit gates. The strength of this coupling is proportional to the level splitting in the absence of a magnetic field, which was found to be an order of magnitude larger in a recent experiment with a three-terminal device [15] compared to two-terminal ASQs [11–13]. An overview of a circuit comprising two TASQs capacitively coupled to a resonator and a transmission line is shown in Fig. 3.

The initialization of the TASQ depends on a concrete realization. In the setup we discuss in this work, one can

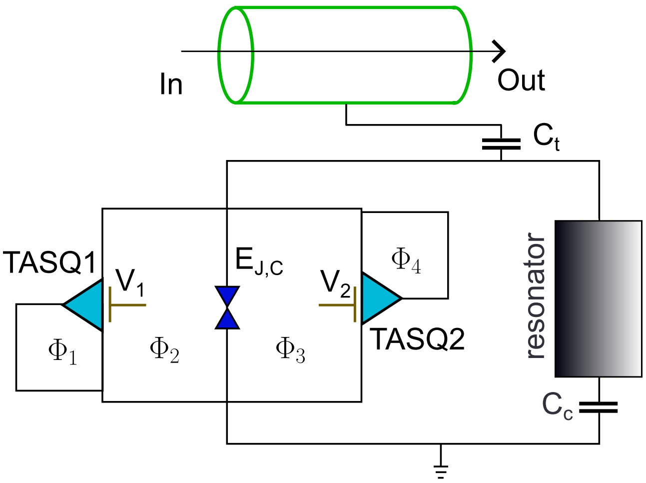

FIG. 3. Diagram of the circuit. Two TASQs are coupled via a superconducting loop with a transmon $E_{J,C}$, and the coupling is controlled by two fluxes Φ_2 and Φ_3. Two additional control loops threaded by the fluxes Φ_1 and Φ_4 are utilized to tune qubit levels. The qubits are capacitively coupled to a resonator (typically LC) via C_c and to the transmission line (in green) via C_t for readout. Two voltage gates V_1 and V_2 under the TASQ1 and TASQ2 allow for the tuning of the qubit levels (DC) and for single-qubit gates (AC).

prepare the system in the odd-parity sector by a resonant microwave drive breaking a Cooper pair and ionizing one quasiparticle to the continuum [38–40]. The initialization can be achieved using the same gate voltage drive. In contrast to two-terminal systems, where the energy splitting between the

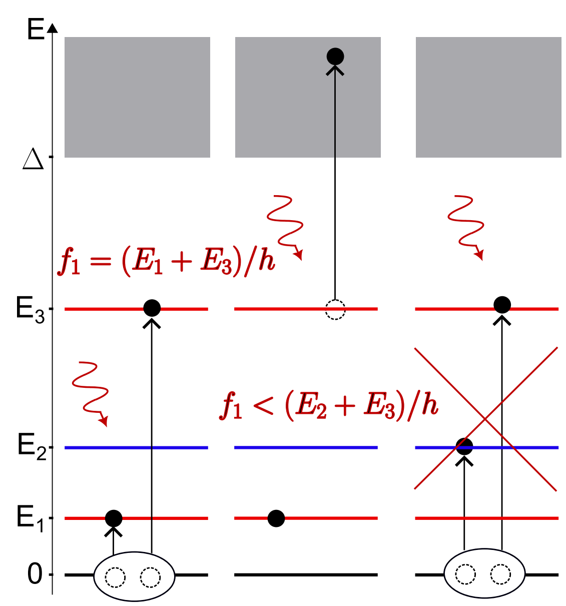

FIG. 4. Details of a resonant two-photon process preparing the qubit in state 1. The frequency of the drive tone is $f = (E_1 + E_3)/h$. Absorption of the first drive photon breaks a Cooper pair populating Andreev levels 1 and 3. Absorption of a second photon ejects the quasiparticle from the upper level into the leads (Δ is the superconducting gap in the leads). Sufficient energy difference between E_1 and E_2 allows for deterministic preparation of the qubit in the desired state.

two lowest-energy states is typically too small to allow for deterministic state preparation, the three-terminal geometry enables a sufficiently large energy difference between the two states with different pseudospin quantum numbers. For example, in the case demonstrated in Fig. 2, a drive at frequency $f_1 = (E_1 + E_3)/h$ populates the first and the third levels with one quasiparticle. If $E_1 + E_3 > \Delta - E_3$, the same drive ionizes a quasiparticle from the higher level into the continuum. Moreover, if $E_1 + E_3 < \Delta - E_1$, a quasiparticle from the first level cannot be excited to the continuum. That provides a condition on the spectrum [39]. This drive is off-resonant with a transition at frequency $f_2 = (E_2 + E_3)/h$, which would prepare the system in the second qubit state. As a result, applying the drive at f_1 provides a deterministic method for initializing the system with one quasiparticle in the first level. The process is summarized in Fig. 4.

It is important to note that thanks to the sufficiently large splitting of the two lowest-energy states in a three-terminal geometry, Coulomb interaction is not required to suppress unwanted transitions back to the even-parity state, unlike in the two-terminal case [38–40]. Consequently, one can choose a drive frequency f_1 or f_2, resonant with the desired transition, to reliably prepare the system in either of the two qubit states.

Conclusions. We have demonstrated, with a microscopic model, the possibility of utilizing a three-lead Josephson junction with SOI as a different type of a qubit—TASQ. Our findings explain recent experimental observations [15] and develop further the ideas proposed in a theoretical work [14]. We demonstrated the possibility to perform all the necessary single-qubit gates and a CNOT gate with two qubits, which is sufficient for universal quantum computing. Furthermore, our theoretical formalism has a great potential for studying new physics of multiterminal superconducting devices, which is a rapidly evolving field of research.

To develop a useful qubit, one needs to create a good model to describe decoherence, as well as ways to mitigate it. Moreover, several different TASQ platforms should be studied, which may require more involved models, including effects such as Coulomb and exchange interactions, disorder, etc. These issues should be addressed in future works.

Acknowledgments. This work has greatly benefited from discussions with Alexander Zazunov, Marco Coraiola, and Alexander Shnirman. K.P. acknowledges funding from Deutsche Forschungsgemeinschaft (DFG; German Research Foundation) Project No. SH 81/7-1. A.S. and W.B. acknowledge support by the Deutsche Forschungsgemeinschaft (DFG; German Research Foundation) via SFB 1432 (Project No. 425217212) and by the Excellence Strategy of the University of Konstanz via a Blue Sky project.

Data availability. The data supporting the findings of this study are available from the corresponding author upon reasonable request. The custom code developed and used for the analyses reported in this manuscript is also available from the corresponding author upon reasonable request.

[1] N. M. Chtchelkatchev and Y. V. Nazarov, Andreev quantum dots for spin manipulation, Phys. Rev. Lett. **90**, 226806 (2003).

[2] M. Veldhorst, J. C. C. Hwang, C. H. Yang, A. W. Leenstra, B. de Ronde, J. P. Dehollain, J. T. Muhonen, F. E. Hudson, K. M. Itoh, A. Morello, and A. S. Dzurak, An addressable quantum dot qubit with fault-tolerant control-fidelity, Nat. Nanotechnol. **9**, 981 (2014).

[3] P. Steinacker, N. D. Stuyck, W. H. Lim, T. Tanttu, M. Feng, A. Nickl, S. Serrano, M. Candido, J. D. Cifuentes, F. E. Hudson, K. W. Chan, S. Kubicek, J. Jussot, Y. Canvel, S. Beyne, Y. Shimura, R. Loo, C. Godfrin, B. Raes, S. Baudot *et al.*, A 300 mm foundry silicon spin qubit unit cell exceeding 99% fidelity in all operations, arXiv:2410.15590.

[4] B. Béri, J. H. Bardarson, and C. W. J. Beenakker, Splitting of Andreev levels in a Josephson junction by spin-orbit coupling, Phys. Rev. B **77**, 045311 (2008).

[5] C. Padurariu and Y. V. Nazarov, Theoretical proposal for superconducting spin qubits, Phys. Rev. B **81**, 144519 (2010).

[6] A. A. Reynoso, G. Usaj, C. A. Balseiro, D. Feinberg, and M. Avignon, Spin-orbit-induced chirality of Andreev states in Josephson junctions, Phys. Rev. B **86**, 214519 (2012).

[7] S. Park and A. L. Yeyati, Andreev spin qubits in multichannel Rashba nanowires, Phys. Rev. B **96**, 125416 (2017).

[8] L. Tosi, C. Metzger, M. F. Goffman, C. Urbina, H. Pothier, S. Park, A. L. Yeyati, J. Nygård, and P. Krogstrup, Spin-orbit splitting of Andreev states revealed by microwave spectroscopy, Phys. Rev. X **9**, 011010 (2019).

[9] M. Hays, V. Fatemi, K. Serniak, D. Bouman, S. Diamond, G. de Lange, P. Krogstrup, J. Nygård, A. Geresdi, and M. H. Devoret, Continuous monitoring of a trapped superconducting spin, Nat. Phys. **16**, 1103 (2020).

[10] A. Bargerbos, M. Pita-Vidal, R. Žitko, L. J. Splitthoff, L. Grünhaupt, J. J. Wesdorp, Y. Liu, L. P. Kouwenhoven, R. Aguado, C. K. Andersen, A. Kou, and B. van Heck, Spectroscopy of spin-split Andreev levels in a quantum dot with superconducting leads, Phys. Rev. Lett. **131**, 097001 (2023).

[11] M. Hays, V. Fatemi, D. Bouman, J. Cerrillo, S. Diamond, K. Serniak, T. Connolly, P. Krogstrup, J. Nygård, A. L. Yeyati, A. Geresdi, and M. H. Devoret, Coherent manipulation of an Andreev spin qubit, Science **373**, 430 (2021).

[12] M. Pita-Vidal, A. Bargerbos, R. Žitko, L. J. Splitthoff, L. Grünhaupt, J. J. Wesdorp, Y. Liu, L. P. Kouwenhoven, R. Aguado, B. van Heck, A. Kou, and C. K. Andersen, Direct manipulation of a superconducting spin qubit strongly coupled to a transmon qubit, Nat. Phys. **19**, 1110 (2023).

[13] M. Pita-Vidal, J. J. Wesdorp, L. J. Splitthoff, A. Bargerbos, Y. Liu, L. P. Kouwenhoven, and C. K. Andersen, Strong tunable coupling between two distant superconducting spin qubits, Nat. Phys. **20**, 1158 (2024).

[14] B. van Heck, S. Mi, and A. R. Akhmerov, Single fermion manipulation via superconducting phase differences in multiterminal Josephson junctions, Phys. Rev. B **90**, 155450 (2014).

[15] M. Coraiola, D. Z. Haxell, D. Sabonis, M. Hinderling, S. C. ten Kate, E. Cheah, F. Krizek, R. Schott, W. Wegscheider, and F. Nichele, Spin-degeneracy breaking and parity transitions in three-terminal Josephson junctions, Phys. Rev. X **14**, 031024 (2024).

[16] M. Alvarado and A. L. Yeyati, 2D topological matter from a boundary Green's functions perspective: Faddeev-LeVerrier algorithm implementation, SciPost Phys. **13**, 009 (2022).
[17] A. Zazunov, A. Iks, M. Alvarado, A. L. Yeyati, and R. Egger, Josephson effect in junctions of conventional and topological superconductors, Beilstein J. Nanotechnol. **9**, 1659 (2018).
[18] M. Alvarado, A. Iks, A. Zazunov, R. Egger, and A. L. Yeyati, Boundary Green's function approach for spinful single-channel and multichannel Majorana nanowires, Phys. Rev. B **101**, 094511 (2020).
[19] S. Pinon, V. Kaladzhyan, and C. Bena, Surface Green's functions and boundary modes using impurities: Weyl semimetals and topological insulators, Phys. Rev. B **101**, 115405 (2020).
[20] V. Kaladzhyan and C. Bena, Obtaining Majorana and other boundary modes from the metamorphosis of impurity-induced states: Exact solutions via the *t*-matrix, Phys. Rev. B **100**, 081106(R) (2019).
[21] A. Komnik and S. Heinze, Analytical results for the Green's functions of lattice fermions, Phys. Rev. B **96**, 155103 (2017).
[22] A. Zazunov, R. Egger, M. Alvarado, and A. L. Yeyati, Josephson effect in multiterminal topological junctions, Phys. Rev. B **96**, 024516 (2017).
[23] Y. Peng, Y. Bao, and F. von Oppen, Boundary Green functions of topological insulators and superconductors, Phys. Rev. B **95**, 235143 (2017).
[24] A. Zazunov, R. Egger, and A. Levy Yeyati, Low-energy theory of transport in Majorana wire junctions, Phys. Rev. B **94**, 014502 (2016).
[25] R.-J. Slager, L. Rademaker, J. Zaanen, and L. Balents, Impurity-bound states and Green's function zeros as local signatures of topology, Phys. Rev. B **92**, 085126 (2015).
[26] L. Arrachea, G. S. Lozano, and A. A. Aligia, Thermal transport in one-dimensional spin heterostructures, Phys. Rev. B **80**, 014425 (2009).
[27] K. Piasotski, N. Müller, D. M. Kennes, H. Schoeller, and M. Pletyukhov, Universal properties of boundary and interface charges in multichannel one-dimensional continuum models, Phys. Rev. B **106**, 165405 (2022).
[28] K. Piasotski, M. Pletyukhov, and A. Shnirman, Green's functions of quasi-one-dimensional layered systems and their application to Josephson junctions, Phys. Rev. B **109**, 014201 (2024).
[29] See Supplemental Material at http://link.aps.org/supplemental/10.1103/55xn-c574 for detailed methods and derivations supporting the main text, including the derivation of the effective Hamiltonian, the calculation of transition matrix elements, and other technical details.
[30] G. V. Graziano, M. Gupta, M. Pendharkar, J. T. Dong, C. P. Dempsey, C. Palmstrøm, and V. S. Pribiag, Selective control of conductance modes in multi-terminal Josephson junctions, Nat. Commun. **13**, 5933 (2022).
[31] E. I. Rashba and A. L. Efros, Orbital mechanisms of electron-spin manipulation by an electric field, Phys. Rev. Lett. **91**, 126405 (2003).
[32] C. Flindt, A. S. Sørensen, and K. Flensberg, Spin-orbit mediated control of spin qubits, Phys. Rev. Lett. **97**, 240501 (2006).
[33] V. N. Golovach, M. Borhani, and D. Loss, Electric-dipole-induced spin resonance in quantum dots, Phys. Rev. B **74**, 165319 (2006).
[34] E. I. Rashba, Theory of electric dipole spin resonance in quantum dots: Mean field theory with Gaussian fluctuations and beyond, Phys. Rev. B **78**, 195302 (2008).
[35] D. P. DiVincenzo, Two-bit gates are universal for quantum computation, Phys. Rev. A **51**, 1015 (1995).
[36] A. Ekert and R. Jozsa, Quantum computation and Shor's factoring algorithm, Rev. Mod. Phys. **68**, 733 (1996).
[37] J. E. Mooij and G. Schön, Propagating plasma mode in thin superconducting filaments, Phys. Rev. Lett. **55**, 114 (1985).
[38] J. J. Wesdorp, L. Grünhaupt, A. Vaartjes, M. Pita-Vidal, A. Bargerbos, L. J. Splitthoff, P. Krogstrup, B. van Heck, and G. de Lange, Dynamical polarization of the fermion parity in a nanowire Josephson junction, Phys. Rev. Lett. **131**, 117001 (2023).
[39] P. D. Kurilovich, V. D. Kurilovich, A. E. Svetogorov, W. Belzig, M. H. Devoret, and L. I. Glazman, On-demand population of Andreev levels by their ionization in the presence of coulomb blockade, Phys. Rev. B **110**, 184508 (2024).
[40] K. Zatsarynna, A. Nava, A. Zazunov, and R. Egger, Many-body quantum dynamics of spin-orbit coupled Andreev states in a Zeeman field, Phys. Rev. B **109**, 214505 (2024).